Electronic Supplementary Material (ESI) for Physical Chemistry Chemical Physics.

Engineering chemical pathways for phase-tuned nanocrystalline Iron oxides in microwave-assisted solvothermal synthesis

Shalini Kandoor, Sukanya Dhar, Lavanya Kumar, Sarath Arackal, Ranajit Sai, and Srinivasarao A. Shivashankar*

Abstract: In Microwave-assisted solvothermal synthesis (MASS) of nanocrystalline iron oxides, we have analysed chemical pathways to explore the role played by temperature and heating rate in deciding phases and crystallographic orientations. We have achieved control over synthesis parameters by using tailored mixtures of solvents. These kinetically controlled pathways are engineered by suitably mixing high microwave dielectric loss solvents – ethanol and water, with 1-decanol. We propose two new pathways, and combinations of different pathways to explain observed phases in reactions between metal acetylacetonates and these solvents, using $Fe(acac)_3$ as a representative. The proposed pathways also explain changes in local geometry from octahedral to square pyramidal, enroute to tetrahedral in oxides. Mixing solvents to alter tanδ is shown to provide an energy-efficient way to control specific geometry of grown phases. The results demonstrate new ways of analysing and tuning synthesis of complex oxides in pure and mixed solvents, under microwave irradiation.

Table of Contents

S1. Experimental Procedures

Please refer to Table 1 of the main text for reference and nomenclature.

$Fe(acac)_3$ (Iron acetylacetonate, Merck, 99%), analytical grade 1-decanol (D, 99%, Spectrochem), ethanol (E, 99.9%, Commercial Alcohols, Canada), and deionized water (Millipore) were used for the experiments. For MASS process in 1-decanol (D), 0.5 mmol of $Fe(acac)_3$ precursor was dissolved in 10 ml of D and the solution was exposed to microwave (2.45 GHz, 300 W) irradiation in a closed system (Discover, CEM Corp., US) with fibre-optic temperature sensor, and 1 cm×1 cm of p-type Si (100) substrate immersed in the solution in 80 ml reaction container. Duration of microwave irradiation (MI) varied from 2 to 40 minutes. After MI, the irradiated solution was cooled to room temperature allowing the precipitates, if any, to settle. The solid precipitate was separated from the organic liquid by centrifuging (15 min, 6000 rpm) and washing the precipitate repeatedly with ethanol and acetone to remove unreacted precursors, if any. The precipitate was then dried at 50 °C for 24 hours, and for powder XRD analysis, grounded to fine powder using mortar and pestle. The films were carefully taken out after the solution was cooled down to room temperature and washed in fresh D twice to remove particles loosely lying on the surface of the film. Finally, the films were blow-dried in N_2 and kept in oven at 50 °C for 1 hr. For growth in ED, 0.5 mmol of $Fe(acac)_3$ was dissolved in 10 ml mixture of decanol and ethanol (D:E = 5:3 in volume), and for DW, 0.5 mmol of $Fe(acac)_3$ was dissolved in a mixture of 10 ml D and 1 ml water (W). Irradiation procedure and post treatment of films/particles were similar to D-system (Table 1).

Particles and films were characterized for structure using X-ray diffractometry (XRD) (Rigaku SmartLab, Cu-Kα radiation) in the normal θ-2θ mode and glancing angle mode, respectively. Relative proportion of Fe^{3+} and Fe^{2+} in the oxide films were obtained from deconvoluting data from X-ray photoelectron spectroscopy (XPS, Kratos AXIS ULTRA). FTIR spectra of irradiated solutions and particles in KBr pellets were obtained (PerkinElmer Frontier spectrometer) in the ATR mode. Identification of organic species in irradiated solution was made using ^1H NMR and GCMS. For these two characterizations, the solutions were centrifuged and celite-filtered multiple times to remove suspended metal oxide/magnetic particles. For NMR analysis, samples were subjected to preparative TLC (thin layer chromatography) in ethyl acetate/hexane (1:9) eluant for isolating the organic compounds from inorganic materials. Organic compounds, along with the stationary phase (silica), were scraped from TLC plate, filtered, washed with $CDCl_3$, and the liquid was submitted for NMR analysis. ^1H (500 MHz) spectra were recorded at room temperature (Jeol-ECZ500) in $CDCl_3$. GCMS was carried out (Agilent 7890A GC system) with auto sampler along with Agilent 5975c TAD inert MSD.

S2. Details of FTIR

Table S1. Absorption band positions, corresponding bond stretching (ν) and bending (δ), and functional groups as obtained from FTIR spectra.

Band Position (cm^{-1})	Band assignments	Functional group	Referred in Fig.
1526 and 1576	ν(C=O) + ν(C=C)	conjugated carbonyl groups of $Fe(acac)_3$	3(a) and (b), S5(a)
1746	ν(C=O)	Ester	3(a) and (b), S5(a)
1236	ν(C-O)	Ester	3(a) and (b), S5(a)
1705–1725	ν(C=O)	Ketone/aldehyde/ester resonance/carboxylic acid/mixture of above	3(a) and (b), S5(a) ester resonance in S1(a)
1705	ν(C=O)	2-Tridecanone	S5(a) and S1(b)
3500 br	ν (O-H)	Decanol	3(a)
1622 br	ν(C=O) + ν(C=C)	Enol form of acacH	3(b)
1648 br	δ(O-H)	Water	3(b)
Various	ν(C-H) and δ(C-H)	Any of the above	3(a)

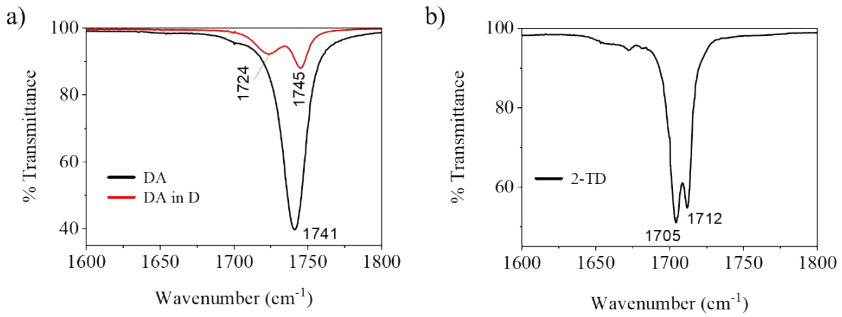

Figure S1. a) FTIR spectrum of neat DA and DA in D (DA:D=1:5 in vol) showing the resonance peak (~1724 cm^{-1}) of ester in alcohol medium due to the H-bonding. b) FTIR spectrum of reference 2-TD showing sharp bands at 1705 and 1712 cm^{-1}. These reference spectra are obtained for the analytical grade reagents using the same FTIR instrument.

S3. Details of NMR

The ^{1}H NMR studies are generally used for the confirmation of structure and purity of an organic compound in a reaction. However, the study carried out in this work is with the intention of confirming the presence of a particular functional group and its local chemical environment, and not for its exact structure, as the reaction mixture expected to consist of more than one organic species. The assignment of characteristic peaks is presented in Table S2 and Figure S2 for D4 and D40. As most of these species consist of aliphatic long hydrocarbon chains, it was necessary to combine the NMR data with the GCMS data to confirm the exact structure of the individual organic species present in the reaction mixture. Though NMR aids in identifying organic by-products in this work, the tedious process of multiple centrifugations and celite filtration, combined with preparative thin layer chromatography (TLC) procedure to remove magnetic iron oxide particles from irradiated liquid, limited its application.

Table S2. Chemical shift (δ, ppm) and the corresponding ^{1}H (underlined) in chemical groups of various species from ^{1}H NMR spectrum of D40 sample. The solvent used is $CDCl_3$ over chloroform.

Band Position, cm-1	Band assignments	Functional group
DA	2.04 (s)	CH_3CO-
	4.05 (t)	CH_2-O-
TD	2.08 (s)	CH_3CO-
	2.41 (t)	-CH_2-CO-
Enone	6.08 (d)	-C(=O)-CH=CH-CH_2-
	6.8 (q)	-C(=O)-CH=CH-CH_2-
Decanal	9.78 (s)	-CHO
Ac	2.13 (s)	CH_3-CO-
Long chain hydrocarbon	0.8 – 1.5	-CH_3, -CH_2-

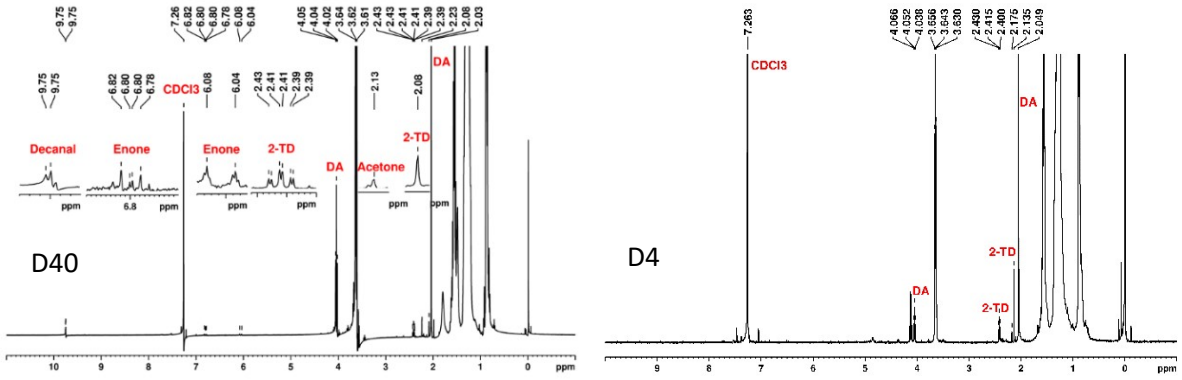

Figure S2. ^{1}H NMR spectra of reaction mixture D4 in comparison to D40, indicating the absence of D-al and En, and a much higher amount of 2-TD at lower time (4 mins) and T.

S4. Quantitative data from GCMS

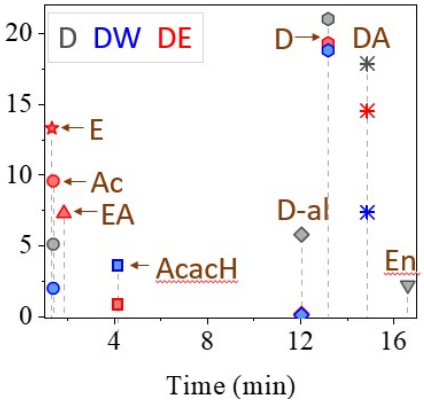

Figure S3. Comparison of GC of reaction mixtures D40, DW40 and DE40. Overlapping peak lines are removed, and self-explanatory symbols correspond to the maximum intensity of each of these peaks.

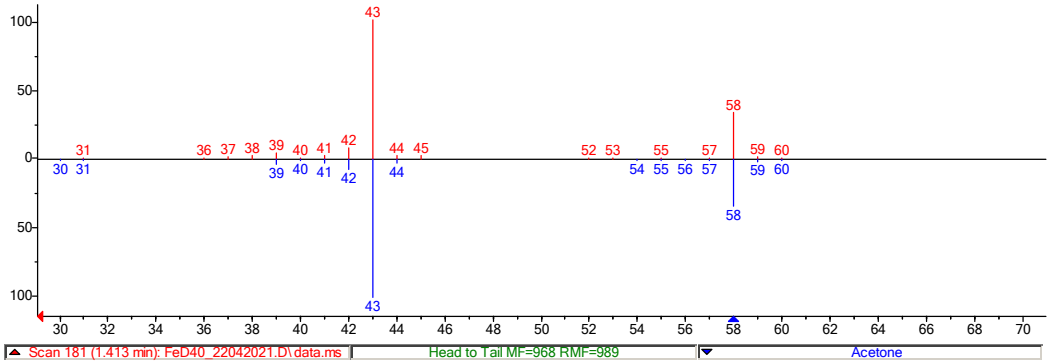

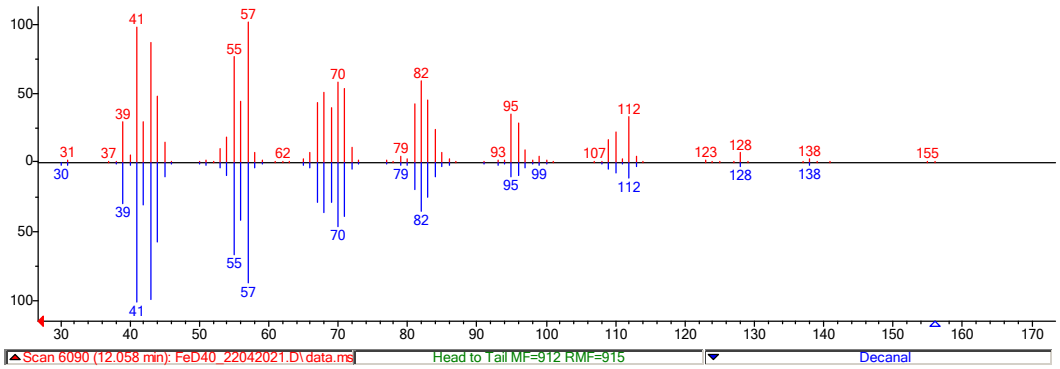

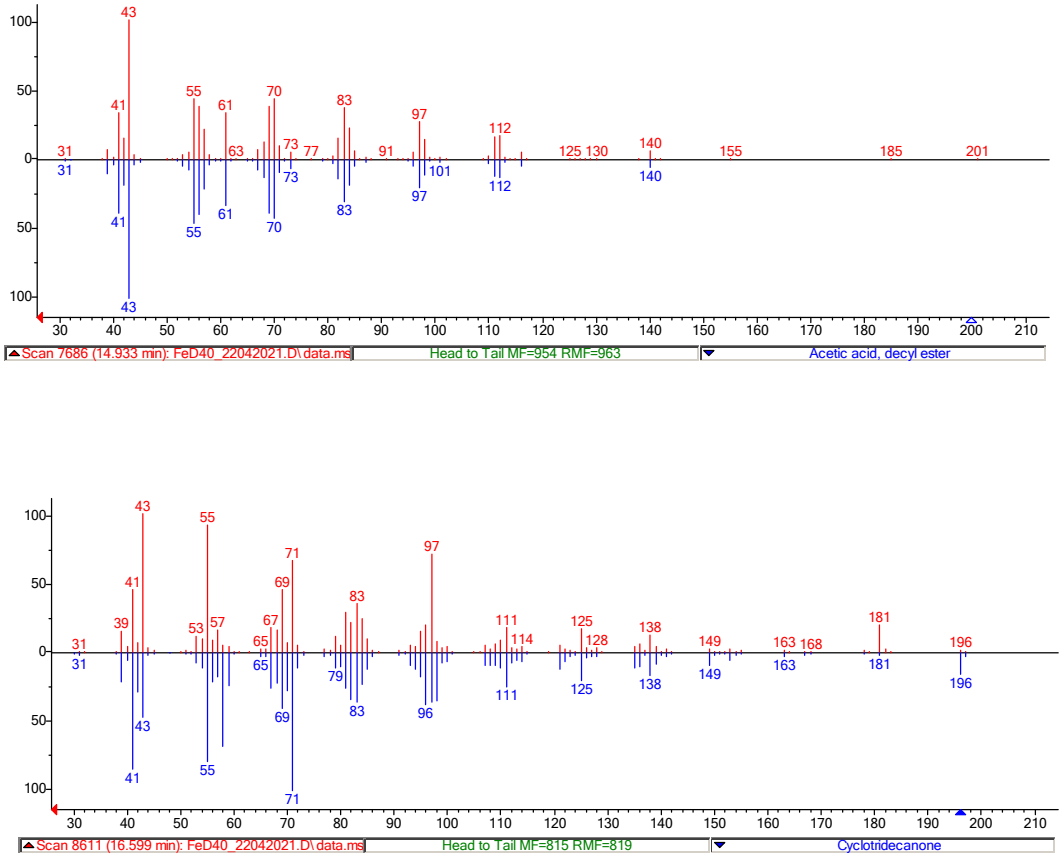

Figure S4. Representative mass spectra of acetone, decanal, decyl acetate, and enone (3-tridecen-2-one) for D40.

Table S3. Ratio of peak intensities of various species from GC spectra of D and DE system.

System	Species	Ratio for	Ratio of peak intensity
D	Enone	D4:D40	1:13
	Decanal	D4:D40	1:15
	DA	D4:D40	1:1.4
	Ac	D4:D40	1:3.3
DE	EA	DE8:DE40	1:3.7

	DA	DE8:DE40	1:6.4

S5. Ester-Ketone Pathway

The mechanism involves a reaction initiation step with formation of decyl acetate (an ester) and 2-tridecanone/acetone (a ketone). In this step, the oxygen atom of decanol brings about a nucleophilic attack on the carbon of one of the C=O groups in the acetylacetone (acac) moiety of $Fe(acac)_3$. This results in the breakage of C-C bond adjacent to the C=O group, resulting in enolate group on one side and the bulky decyl acetate ester on the other side. This ester being weakly attached to the central Fe^{3+} ion by coordinate bond, subsequently breaks away from it into the solution. After the ester elimination, the central Fe^{3+} is coordinately unsaturated and hence it is prone to further reaction. At this stage, the electron-rich oxygen atom of a second D molecule causes nucleophilic attack on Fe^{3+} as shown in the mechanism. In the next step, the enolate group attacks the terminal -CH_2 group in an aldol condensation-type of reaction to form a long chain ketone, i.e., 2-tridecanone. The presence of a small amount of water at this stage, either as moisture absorbed in the starting material or formed during the course of the reaction, results in acetone, as shown. Formation of acetone along with high carbon ketones may be justified because of the higher microwave absorbance and the smaller size of water molecules, offering them easier access to $Fe(acac)_3$ than bulky alcohols.

S6. Details on Pathways Leading to Inorganic Products

The first possible reaction is when all the four acac moieties in the oxo-bridge complex react through the ester-ketone pathway, resulting in $(OH)_2Fe\text{-}O\text{-}Fe(OH)_2$. This species results in Fe_2O_3 through the intramolecular loss of water molecules. The oxide Fe_2O_3 thus formed is predicted to be in the most stable α-form, and is expected when the system dwells long enough at lower T, which is not conducive to the aldehyde and enone pathways.

Alternatively, the $(acac)_2Fe^{3+}\text{-}O\text{-}Fe^{3+}(acac)_2$ complex can undergo two different possible reactions as the temperature is increased, resulting in two oxo-bridge complexes: (1) 3,2-oxo-bridge complex, $(acac)_2Fe^{3+}\text{-}O\text{-}Fe^{2+}(acac)$, when one of the Fe atoms undergoes reduction from Fe^{3+} to Fe^{2+} through the decanal pathway; (2) 3,3-oxo-bridge complex, $(acac)_2Fe^{3+}\text{-}O\text{-}Fe^{3+}{=}O$, when a double bond is directly formed between Fe and O through the enone pathway, without change in the oxidation state of Fe. While the formation of $\alpha\text{-}Fe_2O_3$ through the well-known E-K pathway is expected, the possible reaction pathways for two complexes above, leading to the formation of Fe_3O_4 and $\gamma\text{-}Fe_2O_3$, has not so far been reported. Subsequent reactions of these two complexes yielding different oxides can be explained as below.

The 3,2-oxo-bridge complex, $(acac)_2Fe^{3+}\text{-}O\text{-}Fe^{2+}(acac)$, reacts further via the E-K pathway at both the Fe centres, to form the species $O{=}Fe^{3+}\text{-}O\text{-}Fe^{2+}\text{-}OH$. This species further reacts with O=Fe-OH, an intermediate formed though the enone pathway, to form Fe_3O_4. As the formation of O=Fe-OH involves the reaction of $Fe(acac)_2.OH$ with decanal, it is expected to occur when there is a high concentration of decanal in the reaction mixture. This means that the amount of O=Fe-OH increases with reaction time and hence the reaction temperature. Under these reaction conditions, the enone pathway of single molecular $Fe(acac)_2.OH$ species is more favoured than the self-combination reaction (by E-K route), thereby yielding the bimolecular 3,2-oxo-bridge complex and hence Fe_3O_4.

The 3,3-oxo-bridge complex, $(acac)_2Fe^{3+}\text{-}O\text{-}Fe^{3+}{=}O$, through a similar E-K pathway yields $(OH)_2Fe^{3+}\text{-}O\text{-}Fe^{3+}{=}O$ which, upon intramolecular loss of water, results in the formation of Fe_2O_3. The Fe_2O_3 formed through this sequence of steps is expected to be $\gamma\text{-}Fe_2O_3$. The reason for expecting the γ-phase in the present case, and the α-phase through the 3,3-oxobridge complex mentioned earlier, is explained in the main text.

S7. Necessity of High Temperature for γ-Fe_2O_3

Though the enone pathway is essential for the formation of tetrahedral Fe-O in both Fe_3O_4 and γ-Fe_2O_3, the FeOOH formation through the enone pathway, necessary for Fe_3O_4, involves a single $Fe(acac)_2.OH$ complex (equations 1&2), while the formation of γ-Fe_2O_3 phase predominantly involves the reaction, through the enone pathway, of the originally formed oxo-bridge complex (equation 3). Because of the structural rigidity of this oxo-bridge complex, the change in coordination from octahedral to tetrahedral is difficult to achieve and hence requires a still higher temperature.

$Fe(acac)_2.OH \rightarrow FeOOH$ (through enone pathway) (1)

$FeOOH + (acac)_2Fe^{3+}\text{-}O\text{-}Fe^{2+}(acac) \rightarrow Fe_3O_4$ (2)

$(acac)_2Fe^{3+}\text{-}O\text{-}Fe^{3+}(acac)_2 \rightarrow \gamma - Fe_2O_3$ (through enone pathway) (3)

S8. Time Dependent Study of Organic and Inorganic Species in D, DE and DW

The predominance of a particular pathway over the others at different temperatures determines the resulting oxide phase. Therefore, MI was carried out for different lengths of time (2, 4, 8, 15, 40 min, sample denoted as D2, D4, D8 *etc.* following Table 1 nomenclature in the main text) so as to truncate the reaction at different temperatures and study the resulting organic and inorganic species. FTIR spectra of the reaction mixture after MI for different durations are compared with that of the virgin sample [Figure S5(a)].

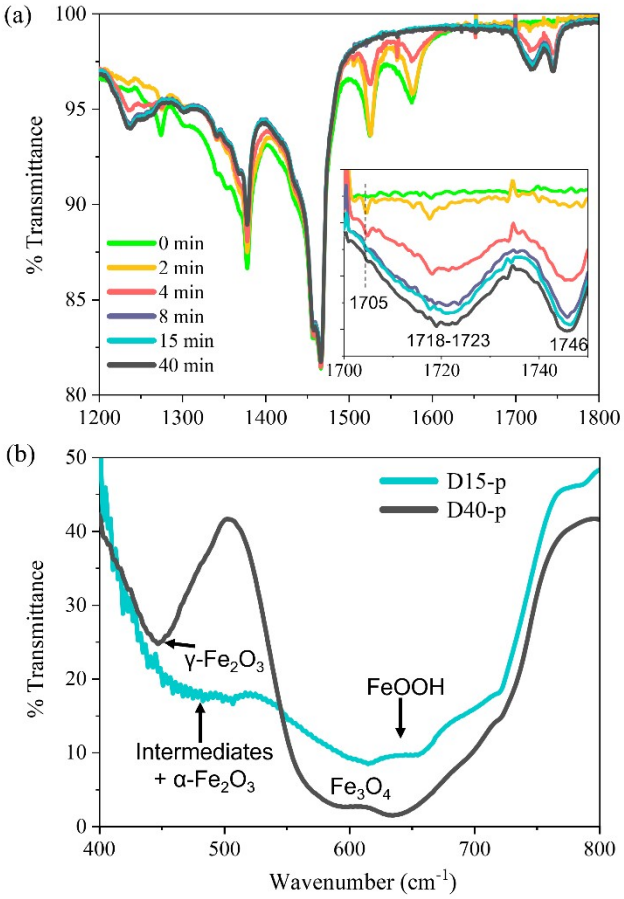

Figure S5. a) Comparison of FTIR spectra of the reaction mixture in D after MI for different durations. b) FTIR spectra of iron oxide nanoparticles in D15 and D40.

The spectra of all samples show characteristic bands in the fingerprint region for esters and ketone/aldehyde, indicating their formation regardless of MI duration. The spectrum of the 2-min sample indicates the onset of reaction by exhibiting bands for DA at 1746 cm^{-1}, and for 2-TD at 1705 cm^{-1}. Reduction in band intensity of 2-TD with MI duration indicates its formation largely during the initial stages of the reaction, after which acetone (Ac) dominates, as water is generated in the medium. The C=C and C=O bands of $Fe(acac)_3$ at 1526 cm^{-1} and 1576 cm^{-1} disappear after 8 min, indicating its complete consumption. The spectra of samples irradiated for 4 min or longer exhibit a broad band in the 1718-1723 cm^{-1} region, indicating merging of Ac, D-al peaks and a resonance peak [~1724 cm^{-1}, shown in Figure S1(a)] of ester in alcohol medium due to the H-bonding[1]. Increase in band intensity of these species with time indicates an increase in their concentration. Similar increase is observed in GC peak intensities of D-al and En with MI duration, suggesting domination of aldehyde and enone pathways at longer durations of MI. The enone pathway is particularly dominant at high T (S7) when there is no available water in the medium. This is evident from the FTIR spectra of D15 and D40 samples [Figure S5(b)]. The oxide phases in D40 are well formed, showing characteristic bands corresponding to Fe_3O_4 and γ-Fe_2O_3. But D15 shows FeOOH[2] as

the only identifiable inorganic intermediate species. This indicates that different metalorganic intermediate species formed during 15 min through aldehyde and enone pathways did not proceed further to form oxides was MI is stopped. The broad bands around 470 cm^{-1} and 600 cm^{-1} may well be due to these intermediates, which could not be readily assigned. A small amount of α-Fe_2O_3 might also be responsible for the 470 cm^{-1} band, which could be formed during cooling from the remnant intermediate $(acac)_2Fe^{3+}$-O-$Fe^{3+}(acac)_2$. During cooling, the water released by the intra- and inter-molecular condensation of the already formed OH groups facilitates the E-K pathway through acetone, and creates $(HO)_2Fe^{3+}$-O-$Fe^{3+}(OH)_2$, which on further loss of water results in α-Fe_2O_3. Disappearance of bands corresponding to these species in D40 validates their intermediate nature, while also implying a temperature >150 °C and irradiation for >15 min is needed for the formation of Fe_3O_4 and γ-Fe_2O_3. Formation of FeOOH and other intermediate species, as well as possible traces of α-Fe_2O_3 in D15, but not in D40, is consistent with the mechanism presented in Scheme 4. The absence of α-Fe_2O_3 in D40 can be explained from the T-profile [Figure 2], which indicates that the system does not dwell for sufficient time at lower T. Hence, aldehyde and enone pathways indicated in Schemes 2 and 3, leading to Fe_3O_4/γ-Fe_2O_3, start before the system settles for α-Fe_2O_3 formation by the ester-ketone pathway. It is also observed that formation of particles is favoured over films in D as the constantly increasing T (Figure 2) is not favourable for film growth.

MI for different durations of time was carried out also for the DE system and the resultant organic and inorganic species were analysed. While both the alcohols (E and D) participate in the reaction initially, D predominates at the later stages of the reaction, as indicated by intensity of GC peaks for DE8 and DE40 [Figure S6(a) and (b), and rows 5 and 6 in Table S3]. However, there is no new species formed at the later stages of the reaction. This further suggests α-Fe_2O_3 as the predominant phase. The temperature profile of DE (Figure 2) also shows that maximum temperature attained is much lower than 150 °C, where only α-Fe_2O_3 is possible. In the XRD pattern of α-Fe_2O_3 for DE40 film [Figure 1(a)], the reflections (104) and (110) have almost equal intensity, indicating no preferred orientation. XRD results are corroborated by XPS [Figure S7], which indicates the presence of only Fe^{3+}, further confirming the α-Fe_2O_3 phase. The formation of only α-Fe_2O_3 is consistent with the prediction of the proposed reaction mechanisms for oxide formation based on organic pathways. The temperature profile for the growth of DE40 (Figure 2) shows that the temperature reaches ~125°C within the first five minutes of irradiation, after which there is a very slow increase of ~10°C at the end of 40 min. Such (relatively) constant temperature is responsible

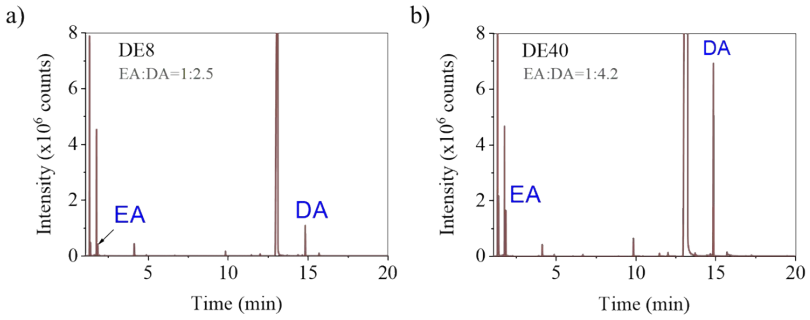

for the preference of growth of films to the particles, as observed in this system.

Figure S6. Gas chromatogram (GC) of (a) DE8, and (b) DE40, providing relative quantitative estimate of organic products. The difference in ratio in EA:DA in 8 and 40 minutes indicates that D predominates at the later stages of the reaction.

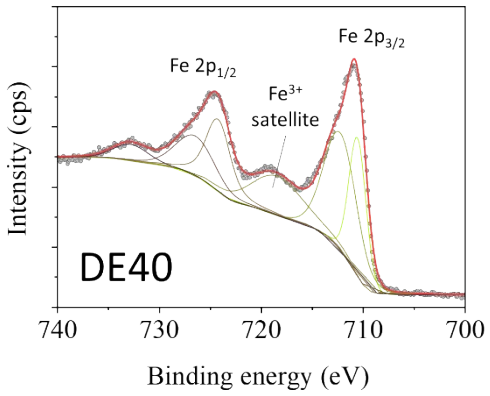

Figure S7. Fe-2p XPS spectrum of DE40 showing only Fe^{3+}.

Similar to DE system, the same phase was observed in DW system for both shorter and longer durations of MI, as indicated in the FTIR data. Particles in DW40 were thoroughly characterized by XRD [Figure 1(a)] and complemented by FTIR [Figure S8(a)] and XPS [Figure S8(b)] and found to be of only the α-Fe_2O_3 phase. T-profile for growth of DW40 (Figure 2) indicates that the rate of increase in T is slower than that in DE40, and T saturates at ~120°C, which is even lower than in the DE system. However, the heterogeneity of D and water is responsible for the predominant formation of particles, possibly by W acting as nucleation sites, resulting in a much thinner film than in the DE and D-systems. These results reaffirm the proposed organic and inorganic pathways to oxide formation.

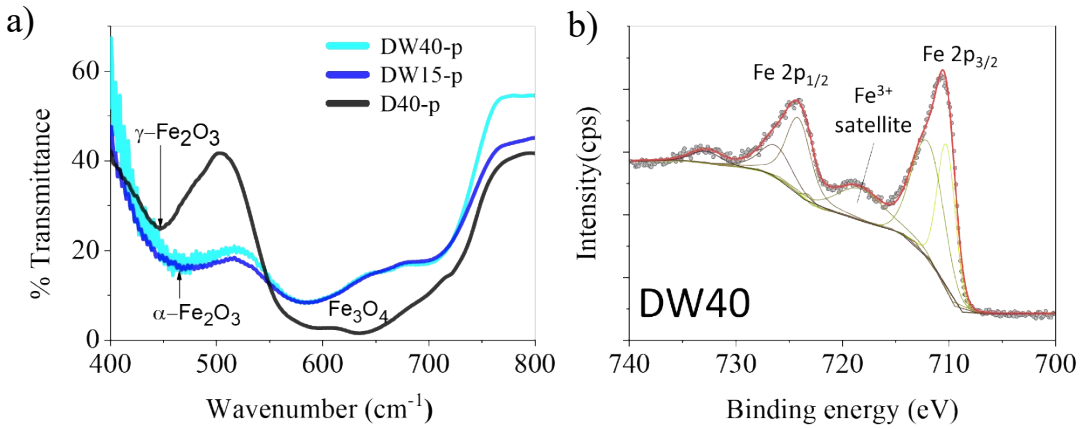

Figure S8. (a) Comparative FTIR spectra of iron oxide particles (as KBr pellets) obtained for DW15 and DW40 showing no change in phase (α-Fe_2O_3) with MI time. Some broad peaks, corresponding to intermediate species, are also observed. Fe_3O_4 and γ-Fe_2O_3 particles obtained in D40 are also shown in contrast. (b) Fe-2p XPS spectrum of DW40 particles showing only Fe^{3+}.

S9. SEM and TEM microstructures of films and particles:

SEM images of films and particles (isolated from liquid after irradiation) obtained by the synthesis in D and DW medium are presented in Figure S9. The images show uniform coverage with different textures of agglomerated particles. Similar images are observed in films grown in DE solvent (Figure 9), where particles in liquid medium could not be isolated. To confirm nano crystallinity of the particles in the film, TEM microstructures of higher magnification were explored for one of the films (DE40), and presented in Figure S10. The images indicate that the particle size is consistent with those obtained in XRD [Figure 1(a)]. As the focus of the present work is on identification of phases, and not on microstructure and particle size, extensive analysis on this aspect was not performed.

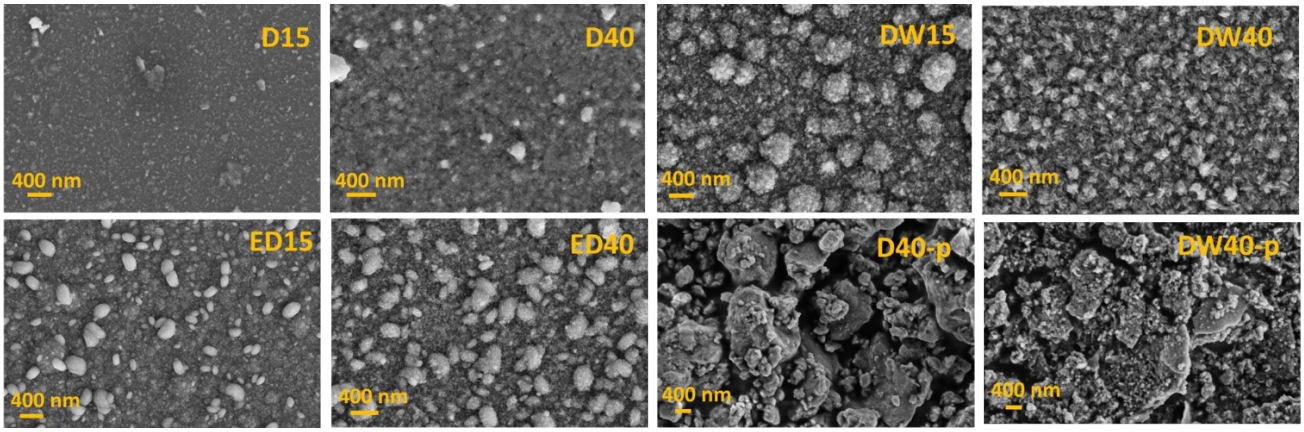

Figure S9. SEM images of films grown for 15 and 40 minutes in D, DW and DE medium, and particles (D40-p and DW40-p) isolated from liquid after 40 minutes of irradiation in D and DW medium.

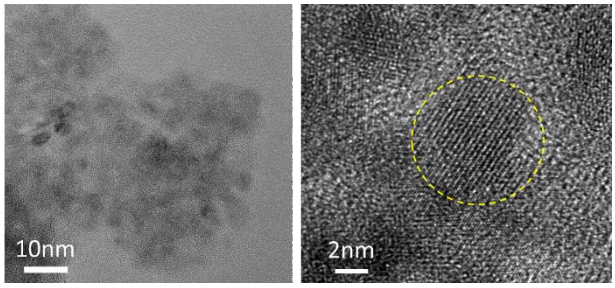

Figure S10. TEM microstructures of DE40 film with higher magnification which confirms nano crystallinity of the particles in the film.

S10. Confirmation for presence of Fe^{2+} ion, to establish Fe_3O_4 formation in D medium

In Figure 1(b), XPS spectra of particles for D40 reveals presence of Fe^{2+} ions, confirming formation of Fe_3O_4. Quantitative analysis of deconvoluted Fe-2p XPS peaks also reveals excess Fe^{3+}, indicating presence of both Fe_3O_4 and γ-Fe_2O_3. As XPS technique is surface specific and is not a representative of the bulk of the material, we have analysed the powder samples (isolated from liquid after 40 minutes of irradiation) grown in D and DW by FTIR for phase identification. FTIR spectra recorded as KBr pellets of D40 samples showed the presence of both Fe_3O_4 and γ-Fe_2O_3 [Figure S5(b)], while in DW medium, only α-Fe_2O_3 is found [Figure S8(a)]. The spectra for the samples grown in D and DW are distinctly different as seen in this comparative spectrum of Figure S8(a). FTIR spectrum of films grown in D also indicates presence of both Fe_3O_4 and γ-Fe_2O_3, as presented in Figure S11(a).

To further confirm the formation of Fe_3O_4 in 1-decanol medium, chemical analysis for the presence of Fe(II) and Fe(III) is carried out (details in next paragraph). The analysis using ammonium thiocyanate test for Fe(III) and potassium ferricyanide test for Fe(II)[3] showed the presence of both Fe(II) and Fe(III) for the samples grown in D, while negligible amount of Fe(II) is found for samples grown in DW. All these combined results of XRD, XPS, FTIR and the chemical tests confirm that a mixture of Fe_3O_4 and γ-Fe_2O_3 is formed in D medium and α-Fe_2O_3 is formed in DW and DE medium.

Details of chemical analysis: For the chemical test, we dissolved iron oxide particles in concentrated hydrochloric acid to form the chloride salt. To test for the presence of Fe(III), we added NH_4SCN solution to this. The solution turned deep red colour of ferric thiocyanate complex $[Fe(SCN)_6]^{3-}$, confirming the presence of Fe(III). The presence of Fe(II) is confirmed by adding potassium ferricyanide to the chloride solution. The resulting solution turned green instead of the dark blue colour of $KFe[Fe(CN)_6]$ as shown below in Figure S11(b). This is due to the presence of both Fe(II) and Fe(III) in the solution as observed for a known mixture of salts of Fe(II) and Fe(III).

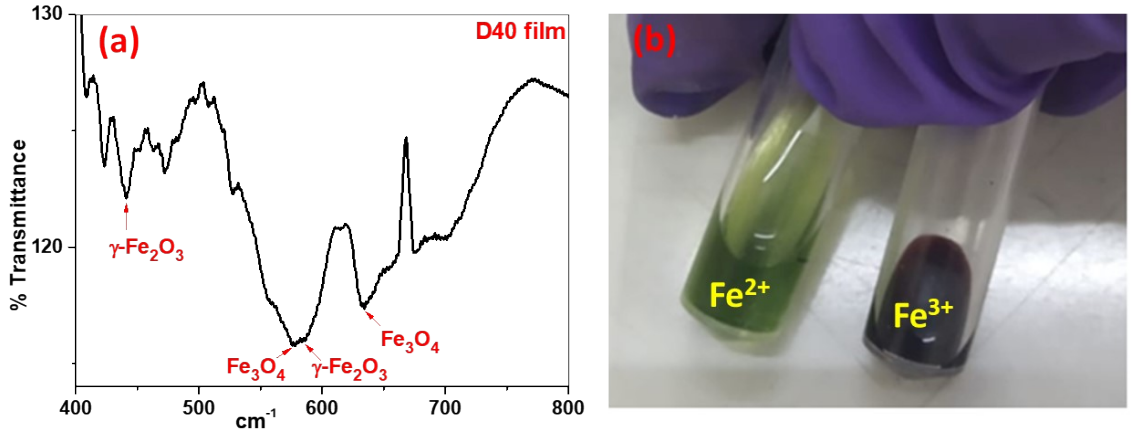

Figure S11(a). FTIR spectrum of D40 film showing Fe_3O_4 and γ-Fe_2O_3, (b) Results of chemical analysis showing presence of Fe^{2+} and Fe^{3+}.

References

[1] J. M. Rodgers, R. M. Abaskharon, B. Ding, J. Chen, W. Zhang, F. Gai, Phys. Chem. Chem. Phys. 2017, 19, 16144–16150.

[2] E. C. Sklute, S. Kashyap, M. D. Dyar, J. F. Holden, T. Tague, P. Wang, S. J. Jaret, Phys. Chem. Miner. 2018, 45, 1–26.

[3] Vogel AI Svehla G. Vogel's Textbook of Macro and Semimicro Qualitative Inorganic Analysis. 5th ed. London: Longman; 1979.

Author Contributions

SK conceived of alternate pathways; SD and SK contributed in data curation, analysis and pathway detection; LK and SA performed experiments (growth and characterization); SK, SD, RS and SAS reviewed data critically in addition to drafting and critically reviewing the manuscript; RS and SAS contributed in funding acquisition.